Journal of Power Sources 588 (2023) 233725

Contents lists available at ScienceDirect

Journal of Power Sources

journal homepage: www.elsevier.com/locate/jpowsour

Quantification of charge carriers and acetate diffusion lengths in intermittent electro-active biofilms using Electrochemical Impedance Spectroscopy

João Pereira [a,b], Yuniki Mediayati [a], Tom Sleutels [a,c], Francisco Fabregat-Santiago [d,*], Annemiek ter Heijne [b,**]

[a] Wetsus, European Centre of Excellence for Sustainable Water Technology, Oostergoweg 9, 8911MA, Leeuwarden, the Netherlands
[b] Environmental Technology, Wageningen University, Bornse Weilanden 9, P.O. Box 17, 6700 AA, Wageningen, the Netherlands
[c] Faculty of Science and Engineering, University of Groningen, Nijenborgh 4, 9747 AG Groningen, the Netherlands
[d] Institute of Advanced Materials, Universitat Jaume I, Av. V. Sos Baynat s/n, 12006, Castelló de La Plana, Spain

HIGHLIGHTS

- Electro-active biofilms were studied using Electrochemical Impedance Spectroscopy.
- Intermittent anode potential regimes were used to study current discharge.
- Current discharge profiles were mainly described by exponential decays.
- EIS showed that current discharge is diffusion limited.
- Concentration of charge carriers was calculated and related to current production.

GRAPHICAL ABSTRACT

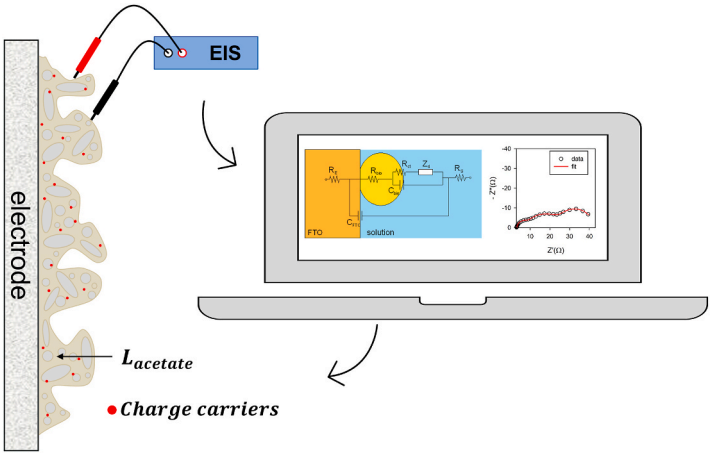

ARTICLE INFO

Keywords:
Electro-active biofilms
Electrochemical impedance spectroscopy
Diffusion limitations
Charge carriers

ABSTRACT

Intermittent anode potential regimes have been used to increase the concentration of charge carriers in electro-active biofilms (EABfs). Even though this increased number of carriers is typically correlated to higher current densities, estimating the concentration of charge carriers in EABfs and linking it to measured current density has never been done. In this study, Electrochemical Impedance Spectroscopy (EIS) and Optical Coherence Tomography (OCT) were used to estimate charge carriers and to study mass transfer limitations in intermittently polarized anodic EABfs. Intermittent potential steps of 20, 60, and 300 s were applied and EABf equilibration times were measured. These times were in the order of 10 s and correlated to the diffusion times obtained from

* Corresponding author.
** Corresponding author.
E-mail addresses: fabresan@uji.es (F. Fabregat-Santiago), annemiek.terheijne@wur.nl (A. Heijne).

https://doi.org/10.1016/j.jpowsour.2023.233725
Received 8 July 2023; Received in revised form 27 September 2023; Accepted 7 October 2023
Available online 17 October 2023

EIS. Acetate consumption rates 100 times faster than the diffusion time of acetate into the EABfs were also estimated with EIS, indicating that current was diffusion limited. Using the capacitance and considering the measured volume of EABf, concentrations of charge carriers ranging from 0.05 $mol_{charge\ carriers}\ m^{-3}_{EABf}$ at current densities of 1 A m^{-2} up to 0.2 $mol_{charge\ carriers}\ m^{-3}_{EABf}$ at current densities higher than 2 A m^{-2} were calculated. This study shows that EIS can be used to study developing EABfs in a non-destructive way and in real-time.

1. Introduction

The ability of electro-active biofilms (EABfs) to exchange electrons with a solid conductive material places them in a very attractive position for engineering applications [1–3]. The combination of EABfs and electrodes is the basis of bio-electrochemical systems (BESs), that have the potential to, among others, recover resources from wastewater and produce added value chemicals [4–7]. The performance indicators of BESs are, among others, linked to the growth and composition of EABfs - the biocatalyst. Therefore, understanding electrochemical characteristics of EABfs and their interaction with electrodes has become of crucial importance for an effective improvement of BESs.

Among the wide range of available techniques to study EABfs, electrochemical techniques are the most used as they allow to analyze the EABfs while they thrive on the electrode [8]. Typically used electrochemical techniques include chronoamperometry that allow to monitor the rate of electrons exchange with the electrode and cyclic voltammetry that indicate the presence of electro-active compounds in EABfs and allows the determination of their formal potential EABfs [9–11]. Besides these examples, Electrochemical Impedance Spectroscopy (EIS) has been suggested as a potential tool to measure and characterize EABfs properties in non-invasive operating settings [12,13]. However, the requirement of a contrasted physic-chemical model represented by an equivalent circuit, that mimics the system under study, and the need for certain expertise to interpret EIS data still raises some arguments among electrochemists, especially when EIS is used to study biocatalysts.

In simple terms, EIS relies on the analysis of a response signal from a given system under study to a controlled input [14]. In electrochemical terms, EIS measurements are taken introducing a small AC perturbation in the voltage (or current), over a system equilibrated at a certain stationary potential. The effect of the perturbation on the current (or voltage) is recorded and used to calculate the impedance. Afterwards, the impedance response is fitted into an equivalent electric circuit, from which electrochemical characteristics such as capacitances, charge transfer and electric resistances can be derived and associated to specific physical-chemical characteristics of the system under study [14,15]. Therefore, this in-situ and non-destructive technique can be applied to EABfs, and through a realistic equivalent electric circuit, provide information about the electrode-EABf interphase, the concentration of charge carriers in the EABf and study how they respond to a set of operating conditions over time. In this work, the equivalent electrical circuit shown in Fig. 1a was used for a complete electrochemical characterization of EABfs. This circuit has previously been validated in a bio-electrochemical system with the same configuration as used here, and it presents the same three arcs observed in Fig. 1b [15]. Briefly, this circuit is an ensemble of electrical components that mimic the different processes occurring in the EABfs, in the electrode, at the interphase electrode and EABfs, and in the anolyte.

This circuit consists of the electric resistance of the electrode (R_{FTO}) - in this case, a transparent conducting Fluorine doped Tin Oxide (FTO), being though also valid for any other conducting electrodes - and its capacitance (C_{FTO}) – which is a measure of the stored charge at the interphase between the electrode and the electrolyte (so-called solution, or anolyte in the case of an anode compartment). In the same line of thinking, R_{bio} represents the resistance which is linked to the transport of electrons in the EABf plus the charge transfer at the interphase between the EABfs and the electrode whereas C_{bio} represents the capacitance which is associated to the amount of charge carriers (i.e., redox compounds like cytochromes) on the extracellular membrane of the cells present in the EABfs. C_{bio} combines the double layer capacitance at the interface of the active parts of the biofilm with the solution, with the chemical capacitance (or pseudo-capacitance) associated with the increasing states available for the carriers. The direct relationship found between the current and C_{bio} in previous work [15] indicates that chemical or pseudo-capacitance contribution is the one governing this parameter. At the interphase between the EABf and the solution (or anolyte), a resistance is represented which relates to the transfer of charge from the biological oxidation of the substrate to the redox carriers - charge transfer resistance (R_{ct}). As such, this resistance is related to the rate of substrate consumption. Finally, a diffusion element, associated to the diffusion of acetate and protons in the electrolyte given by

$$Z_d = R_d \frac{tanh\ [j\tau_d\omega]^{1/2}}{[j\tau_d\omega]^{1/2}} \quad \text{Eq.1}$$

with j, the imaginary number, $\tau_d = d^2/D$, with D representing the diffusion coefficient of these species, d the width of the diffusion layer, and R_d the diffusion resistance in this layer, and a solution resistance (R_s), related to ionic transport in the bulk of the anolyte, are also included. As a note, it is relevant to mention that these different

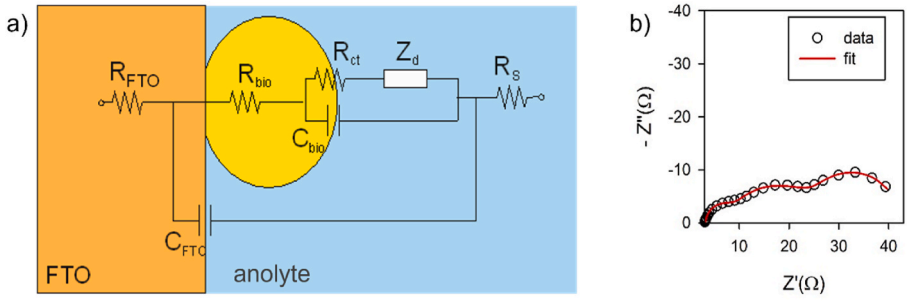

Fig. 1. (a) Schematic overview of the equivalent electric circuit of the assembly Fluorinated Tin Oxide (FTO) electrode (orange) with an EABf (yellow) in the anolyte (blue) to interpret EIS data, and (b) example of the EIS experimental data (dots) and the fitting to the equivalent circuit shown in a) (line). In brief, the impedance spectrum is displaced from the origin by the value of the total series resistance (= $R_{FTO} + R_s$), the high frequency arc corresponds to the parallel combination of C_{fto} and R_{bio}, the intermediate frequency arc to C_{bio} and R_{ct}, and the low frequency arc to the diffusion impedance Z_d. (For interpretation of the references to color in this figure legend, the reader is referred to the Web version of this article.)

processes are only distinguishable when their characteristic frequencies are separated enough to allow the decoupling of the responses of the different phenomena occurring in the assembled BES. Specifically, for EABf growing on an electrode, this requires the use of electrodes with low capacitance (details can be found elsewhere [15]. Even though this circuit has successfully been reported to quantify the capacitance of EABfs and relate the electric components of the circuit with the performance of anodic EABfs grown under a continuous anode potential regime, more information can be gained on the electrochemical characteristics of EABfs by extending the use of EIS to study EABfs under intermittent anode potential regimes.

EABfs can grow under intermittent anode potential regimes, which consist of applying consecutive steps between a fixed anode potential and Open Cell Potential (OCP), and are consequently referred to as intermittent EABfs. In the fixed anode potential period, electrons are transferred to the anode, whereas in OCP, no electrons are exchanged with the anode, resulting in the accumulation of electrons in the EABfs (in other words, EABfs become charged). The interest in EABfs that grow under an intermittent anode potential has increased due to the claimed higher current densities measured at the anode, which are linked to an overproduction of charge carriers (e.g. c-type cytochromes) found in the EABf matrix, which is likely to increase their electron storage capacity, so-called capacitance [16,17]. However, this concentration of charge carriers is typically measured as endpoint analysis as the quantification methods such as spectroscopy, gel electrolysis, or analysis of proteins with standards colorimetric kits are destructive. This is where EIS can contribute with its non-invasive nature and allow for a real-time monitoring of the capacitance and the concentration of charge carriers as EABfs are developing on the anode. This way, capacitance (C_{bio} and also R_{ct}), could be used as an indirect assessment of the EABf activity on the anode by relating it to the measured current density.

Besides allowing to explore the relationship between current density and the capacitance in intermittent EABf, mass transfer limitations can also be studied with EIS. Acetate limitations have been reported for EABfs that grow on anodes and shown to play an important role in EABfs performances [18–20]. These are linked to a limiting diffusion of substrate (e.g., acetate) in the EABf and products (e.g., protons) out of the EABfs, while EABfs grow on the anode. Even though this has been reported for EABfs grown under a continuous anode potential by means of mathematical models [21,22], the study of mass transfer limitations in intermittent EABfs is an unexplored field. Given the different morphologies and higher amount of extracellular polymeric substances (EPS) in intermittent EABfs [23,24], mass transfer limitations are also likely to happen and limit the discharging of the electrons towards the anode after OCP periods. This can be measured with the diffusion resistance element of the equivalent electrical circuit used to fit EIS data and used to calculate the diffusion length of acetate inside the EABfs. With this parameter and the capacitance of EABfs, which can both be monitored over time, the concentration of charge carriers in the EABf can be calculated and thus be related to the current density in real-time under a wide range of conditions.

In this work, we used EIS for a better understanding of the electrochemical response of acetate fed EABfs grown under intermittent potential regimes. The capacitive and diffusive discharge behaviour were studied at three different intermittent times. Acetate diffusion limitations were identified in all the intermittent times used to grow EABfs, and the concentration of charge carriers in the EABfs was calculated and related to the produced current. This work shows that EIS can thus be used to study EABfs and as a tool to identify diffusion limitations.

2. Materials and methods

2.1. Reactor design and setup configuration

The bio-electrochemical reactors were composed of two flow channel compartments (33 mL each, with an operating area of 22.3 cm^2) separated by a bipolar membrane (Ralex PEBPM, MEGA a.s., Czech Republic). A bipolar membrane, with the anion side oriented towards the anode and the cation side oriented towards the cathode, was used to allow the migration of protons to the cathode compartment and hydroxyl groups to the anode compartment. The FTO electrode was used as anode and a graphite sheet, placed in contact with the FTO electrode, was used as current collector. Besides being a glass and flat electrode, the FTO electrode has low capacitance that allows to distinguish the electrode capacitance from the EABfs capacitance. In the cathode, a flat platinum/iridium coated titanium plate (Pt/IrO_2 80:20, Magneto special anodes BV, Schiedam, The Netherlands) was used as counter electrode. This reactor design is described in more detail in [25].

The EABfs were grown on FTO electrodes in a chronoamperometric mode, being the anode potential controlled by a potentiostat (N-stat d-module, Ivium Technologies, Eindhoven, The Netherlands) and the current monitored over time. A three-electrode configuration was used, being all potentials expressed versus an Ag/AgCl electrode (+0.203 V vs. standard hydrogen electrode; Prosense, Oosterhout, The Netherlands). This reference electrode was positioned in between the FTO electrode and the bipolar membrane and connected by means of a Haber–Luggin capillary filled with 3 M KCl solution. The anode compartments of the bio-electrochemical reactors were hydraulically connected to a feed pump (Masterflex L/S, Cole-Parmer, Barendrecht, The Netherlands) to guarantee a continuous flow of fresh influent (23 h hydraulic retention time, given the 220 mL total volume of the reactor with piping and mixing vessels and the used pumping rate of 0.16 mL min^{-1}), and both the anode and cathode compartment were connected to a recirculation peristaltic pump (60 mL min^{-1}) to guarantee homogeneity in both flow channels. During the runs, the bio-electrochemical reactors were kept in a climate chamber with the temperature controlled at 298 K.

2.2. Inoculation and media composition

A mixed culture of acetate fed anodes from previous BESs was used to inoculate the bio-electrochemical reactors in this study. The anolyte was prepared adapting the standard DSMZ culture medium 141, and it constituted of (g L^{-1}): 0.82 $NaCH_3COO$ (10 mM acetate), 3.40 KH_2PO_4, 4.35 K_2HPO_4, 0.1 $MgSO_4.7H_2O$, 0.74 KCl, 0.58 NaCl, 0.28 NH_4Cl, 0.1 $CaCl_2.2H_2O$, 1 mL of trace metals mixture and 1 mL of vitamins mixture [26]. 1.97 g L^{-1} of $BrCH_2CH_2SO_3Na$ was also added to the medium to inhibit methanogenesis and to allow to study and electrochemically characterize the EABfs with EIS. Besides, anaerobic conditions were guaranteed by continuously sparging nitrogen before and during the experiments into the feed bottles before the influent was pumped into the reactor. A 50 mM potassium phosphate buffer solution at pH 7 was added to the catholyte, to which nitrogen was also continuously being sparged to avoid hydrogen build-up and diffusion to the anode.

2.3. Experimental design

The influences of the intermittent anode potential regime and the different intermittent times on the electrochemical characteristics of EABfs, such as capacitance, charge transfer and diffusion resistances were tested. Intermittent times of 20, 60, and 300 s (closed and open circuit times were the same, meaning a duty cycle of 0.5) were applied, and anode potential steps varied from OCP (~−0.44 V vs Ag/AgCl) and a fixed anode potential of −0.35 V vs Ag/AgCl. An acetate concentration of 10 mM was added to the feed to guarantee that the EABfs were not acetate limited. Even though the low overpotentials (the biological acetate oxidation potential is approximately −0.5 V vs Ag/AgCl), the chosen range of low anode potentials in this study is required to achieve acceptable voltage efficiencies in a Microbial Fuel Cell. In short, this translates into higher energy efficiencies, and it means lower energy input to produce hydrogen in a Microbial Electrolysis Cell. After inoculation, the reactors run for approximately 30 days and the EIS measurements were performed after day 5 to avoid interfering with the

initial growth phase of the EABf on the electrode. All conditions were tested in triplicate.

2.4. Chemical, electrochemical, and visual analysis

The reactors were sampled every two or three days to quantify the concentration of acetate in the influent and effluent, to perform EIS measurements, and to measure the thickness of the EABfs. Acetate concentration was measured using Ultra-High-Performance Liquid Chromatography (UHPLC) (300 × 7.8 mm Phenomenex Rezex Organic Acid H+ column, Dionex ultimate 3000RS, Thermo Fisher Scientific, The Netherlands) after sample filtration through a 0.45 μm pore-size filter (EMD Millipore SLFH025NS, Barendrecht, The Netherlands).

EIS measurements were performed using an Autolab PGSTAT302 N potentiostat equipped with a frequency analysis module (Metrohm, The Netherlands). These measurements were performed after the fifth day of EABf growth on the anode, with the ultimate aim of relating EABf thickness with EIS data. Therefore, EIS was used at different EABf thicknesses, and thus produced currents, within replicates to have C_{bio} and R_{bio} data over a wider range of thicknesses and current densities. To assess all the processes described in Fig. 1a, an AC signal with an amplitude of 10 mV was applied in a frequency range of 10 kHz to 5 mHz. During the EIS measurements, only the IVIUM potentiostat used for the chronoamperometric control was disconnected from the reactors, being the influent and recirculation pumps kept on. The fitting of the EIS data to the equivalent electric circuit was done using Zview software. The fitting of the EIS data to the equivalent electric circuit was done using Zview software. Before the first fitting, the high frequency intercept of impedance spectrum was read and the size of the arcs was estimated to determine initial values of the total series resistance, R_{bio}, R_{ct}, and R_d. For the capacitances, a bode plot of the real part of the capacitance is used to read the provided value at high frequency to C_{FTO} and the value at medium-medium/low frequency which serves as initial value of C_{bio}. As an alternative to C_{FTO}, an initial value can be estimated by multiplying 10 μF cm^{-2} by the area of the electrode. The initial value of τ_d can be estimated by multiplying the value of the capacitance read in the bode plot at the lowest frequency by the estimated value of R_d. Once the initial values are introduced in the model selected for the fitting of the spectra (Fig. 1a), the Zview procedure is run without constraints. The result is revised to check for validity according to some assumptions: i.e. total series resistance matches the high frequency intercept of the spectrum, and the sum of all the resistances provides a value close to the low frequency intercept of the spectra.

To relate the EIS data to the current profiles obtained with the IVIUM potentiostat, Sigmaplot software was used. A "steady state" current was defined (and used in the results section) as the last current density measured before the start of the OCP period. For the derivation of the discharging times of the EABfs from the current profiles, the current was recorded every second. The fitting and the derivation of the characteristic time decays were done using four different transients measured for each EABfs after the EIS was performed. Besides, to evaluate whether the use of EIS was invasive to the EABfs, the discharging currents before and after the EIS measurements were compared, as well as the current measured with the IVIUM potentiostat was compared to the current measured during the EIS measurement. No significant changes in the discharging currents were found after EIS measurements nor between the currents measured with the potentiostat and during EIS measurements. More information can be found in Figures A1 and A2, in Appendices.

The thicknesses of the EABfs on the anode were measured over time with Optical Coherence Tomography (OCT). OCT is a technique that uses near infrared light and studies the scattering of light with an interferometer [27]. In this measurement that lasts for 45 min, the electrode on which the EABf grows is scanned in 54 evenly distributed spots and, subsequently, the images are processed with Matlab to calculate the volume (and thickness) of the EABfs. A detailed explanation of this methodology is given elsewhere [25]. The EABf thicknesses on the FTO electrode were measured after EIS measurements, which was first followed by a period of at least 45 min in which the anodic EABfs were intermittently potential controlled, before the OCT measurements.

3. Results and discussion

3.1. Discharging behavior of intermittent EABfs

The intermittent anode potential control of EABfs allows to study how the EABfs discharge once the anode is repolarized after a period of open circuit. The produced current (I) combines a discharging behavior – so-called transient behavior (I_t), after which an approximately constant faradaic current (I_F) can be measured (Equation (2)).

$$I = I_t + I_F \quad \text{Eq.2}$$

In most cases, particularly for repetitive measurements, the current associated to the transient is given by a decay that follows an exponential trend (Equation (3)).

$$I_t = I_0 \, exp\left[-\frac{t}{\tau_t}\right] \quad \text{Eq.3}$$

where I_0 is the onset current and τ_t is the characteristic transient time to charge/discharge the EABf in the intermittent measurement. If the current is monitored at high resolution (in other words, if the measurements are made fast enough), two different characteristic times can be observed in the transient behaviour, which are associated with two types of electron exchange between the EABfs and the anode (Fig. 2): the relaxation transient (τ_{bio}) and diffusive transient (τ_d).

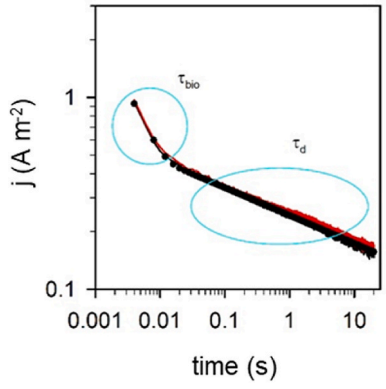

Fig. 2. Example of the two different types of transients observed during a 20 s intermittent EABf discharge after a 20 s OCP period: fast/relaxation transient (τ_{bio}) and slow/diffusive transient (τ_d).

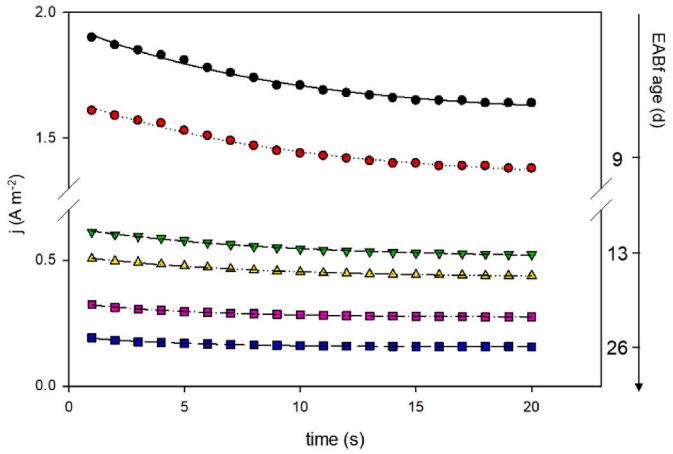

Fig. 3. Example of the discharge of a 20 s intermittent EABfs after an OCP period (current density as a function of time, represented by the datapoints) and the fitting to Equation (3) (lines over the datapoints) to derive the discharging times during the aging of an EABf with decreasing produced current densities over time (vertical axis indicating the age of the EABf).

At the shortest times (in the order of miliseconds), the transient time is faster (as the slope of the transient is steeper), and it is associated to the charge accumulated in the EABf – this fast transient time is referred to as relaxation time (τ_{bio}). Impedance analysis using the model provided in Fig. 1a allowed to corroborate this fast decay to the discharging of the capacitance C_{bio}, associated to charge accumulation in the cytochromes through the internal resistances of the EABfs as given in Equation (4) [14,15]. More details can be found in Figure B1, in Appendices.

$$\tau_{bio} = (R_{FTO} + R_{bio}) \times C_{bio} \quad \text{Eq.4}$$

At the longest times (in the order of seconds), the charge exchange is dominated by the diffusion of charge carrying species: carbon source (in this work, acetate) that diffuses inside the EABf, and products such as protons that diffuse out of the EABf. In the impedance analysis with the model of Fig. 1a, this characteristic τ_d is given by the diffusion element Z_d, as shown in Equation (1).

Diffusion is the process that, at a longer time interval and as thick EABf develop on the anode, determines the produced current by EABfs and the acetate consumption, as it has already been shown for EABfs that grow under continuous anode potential regimes [19,28,29]. Therefore, in this work, focus was given to the transient analysis in the long times decay using Equation (3). Fig. 3 shows examples of the fitting of Equation (3) to the measured discharging currents at different EABf growth stages.

The characteristic time for long times obtained from the transient decays was comparable to the diffusion times of species in the anolyte calculated from the diffusion element (Eq. (1)), obtained from the fitting of EIS measurements (Fig. 4).

These long decay times mainly ranged between 8 and 15 s, which were approximately 100 times slower than the fast capacitive decay. The relationship between the long decay and the capacitive decay calculated with EIS using Eq. (4) can be found in Figure B2, in Appendices.

An exponential decay of the transient associated to diffusion suggests that mobile ions in the anolyte affect the charge density profile of the EABf [30]. After the transient, the measured faradaic current is related to the consumption of the acetate in the EABf. Therefore, the current is determined by the acetate availability in the EABfs, which in turn, is linked to the diffusion of acetate molecules inside the EABfs. Consequently, the overall performance of EABfs can be affected by diffusion processes in the EABfs [19,21,31]. As opposed to the anode potential controlled condition, it is important to note that at OCP there is no diffusion limitation as there is no current, therefore the electrochemical equilibrium is reached very quickly.

It should be mentioned that some discharging profiles did not follow the transient described above. This happened in some discharges of EABfs that were kept at OCP for 300 s, in which an oscillatory behavior was obtained during discharging rather than an exponential decay (Figure B3, in Appendices). This is likely to be related to the longer

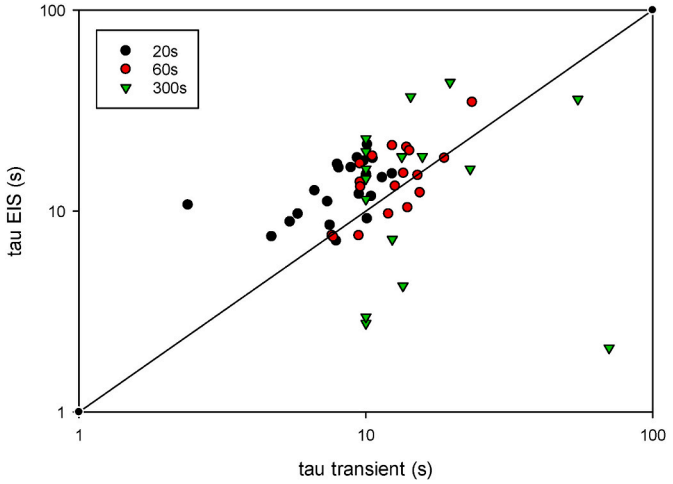

Fig. 4. Discharging times from EIS and transients for all the replicates in the 20, 60, and 300 s intermittent time experiments: similarity between diffusion times (from EIS) and diffusion times calculated from the transients (Eq. (3)) indicates the produced current is diffusion limited.

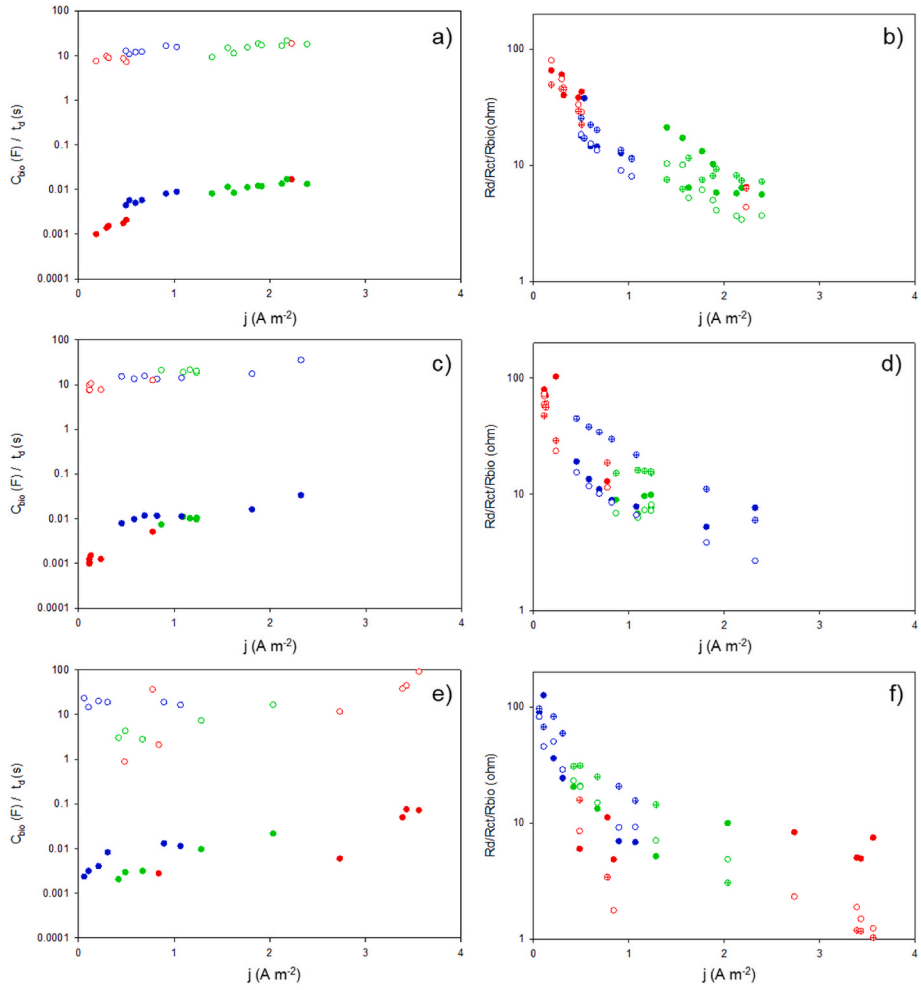

Fig. 5. Capacitance (C_{bio} in F, filled circles), slow decay time (τ_d in s, open circles) and resistances (R in ohms: R_d filled circles, R_{ct} in open circles, and R_{bio} in crossed circles) as a function of the current density for the a) and b) 20, c) and d) 60 and e) and f) 300 s intermittent polarizations of the EABfs (triplicates are shown in green, blue and red). C_{bio} and τ_d increased while the resistances decreased at higher current densities. (For interpretation of the references to color in this figure legend, the reader is referred to the Web version of this article.)

stabilization times when shifting from a real steady state at open circuit to the intermittent potential control in combination with the presence of EPS (their slimy matrix can affect the electron transport and transfer between the charge carriers in the EABf and the anode) and the patchy EABf morphologies [23]. Particularly, when cells are embedded in polysaccharide enriched EPS, these sugars can have an insulating

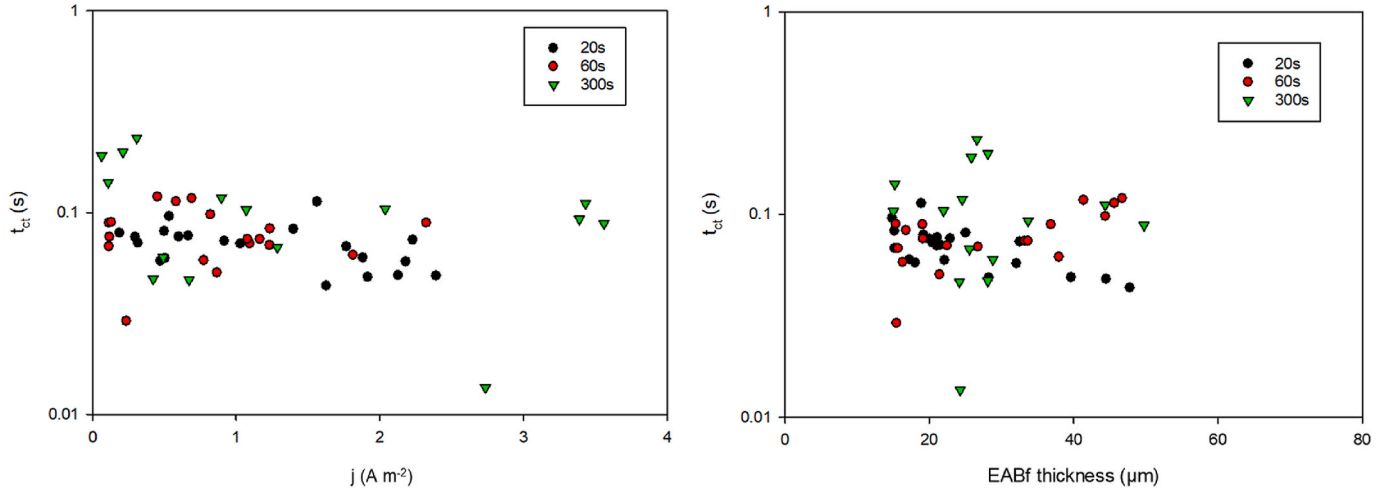

Fig. 6. Acetate consumption rate ($\tau_{ct} = 1/k$, in s) as a function of a) the current density and b) the measured EABf thickness on the anode for all intermittent times tested. The acetate consumption rates were roughly constant and did not relate to the measured current density or the EABf thicknesses.

behaviour, and thus, slow down overall electron transport and transfer rates [32]. These morphological and compositional changes in the EABf as a function of the intermittent anode potential regime may influence the dynamic of charges and lead to wider discharging times and vibrational behaviors.

3.2. R_d, R_{bio}, and R_{ct} decrease with higher current densities whereas C_{bio} and τ_d increase with higher current densities

Fig. 5 shows the capacitances, discharging times, and resistances in the anodic EABfs obtained from the impedance spectroscopies of three independent experiments for each of the intermittent times tested in this study. The general trend shows that higher current densities were obtained when the resistances decreased and when the capacitance of the EABfs increased. These relationships have already been described for continuous EABfs [15], and are here also validated for intermittent EABfs.

For all the intermittent times tested, an increase in the produced currents was related to an increase in the C_{bio}. The highest EABf capacitance was obtained for one of the replicates with the longest intermittent time. Even though the acetate consumption during the OCP period was not measured, it is likely this EABf replicate consumed more acetate during OCP, resulting in the reduction of more charge carriers (due to an increase in the number of charge carriers), and therefore leading to higher current densities and higher capacitances. With higher C_{bio} also longer discharging times were obtained. Again, this was coherent with the presence of more charge carriers in the EABfs and with a higher acetate consumption, resulting in longer times for the oxidation of these carriers by giving the electrons to the anode (longer decay times). As previously reported for continuous EABfs [15], higher current densities are associated to higher C_{bio} and lower charge transfer and transport resistances in the EABf, which are linked respectively, to higher acetate consumption and to a better charge exchange between the EABf and the anode. Besides, the diffusion resistance also decreased with higher current densities, meaning that the diffusion improved at higher current densities. However, in all the anodic EABfs studied, there seemed to be a lower limit for R_d at around 7–8 Ω, which was the smaller resistance reached at the higher anodic current densities for all the intermittent times.

The range of capacitances and resistances reported here for intermittent EABf were in the same order of magnitude as the ones previously reported for continuous EABfs studied on FTO electrodes (C_{bio} up to 0.4 mF cm^{-2} and conductivities between 4×10^{-4} and 4×10^{-2} Ω^{-1} cm^{-2}). However, due to the higher current densities obtained in this study – resulting in higher C_{bio} (up to 4 mF cm^{-2} for the 300 s intermittent EABfs) – it became clear that the increase in C_{bio} as a function of the measured current density becomes more scattered and that the slope C_{bio} vs current density decreases at higher current densities, indicating that a maximum C_{bio} is reached. Finally, these results suggest that either due to R_d or to the availability of charge carriers in the EABfs (indicated by C_{bio}), there is a limitation for more acetate consumption and therefore, for higher current output.

3.3. Acetate consumption kinetics, diffusion length, and EABf thickness

Besides the diffusion time, the diffusion length was also calculated to estimate the EABf thickness that had access to acetate and therefore, to understand whether diffusion was limiting the produced current by the intermittent EABfs. For this purpose, assuming the kinetics of the acetate consumption reaction is of first order, the rate transfer of acetate to electrons, τ_{ct} (which is the acetate conversion rate given by k, s^{-1}), can be calculated from C_{bio} (in F) and R_{ct} (in Ω) using Equation (5).

$$\tau_{ct} = \frac{1}{k} = C_{bio} \times R_{ct} \quad \text{Eq.5}$$

The electron transfer time from acetate oxidation was nearly constant with values of $\tau_{ct} \sim 0.1$ s, which provided a rate of acetate consumption of $k \sim 10$ s^{-1} for all the intermittent EABfs. As these rates were very similar for all the intermittent EABfs, there was no clear relationship between these rates and produced currents or the measured EABfs thicknesses on the anode (Fig. 6). More details can be found in Figure C1, in Appendices. These values are in line with previously reported acetate kinetics of 13 s^{-1} obtained for EABfs that were discharged at +0.2 V vs Ag/AgCl after OCP periods that lasted for 5, 10, 20, and 45 min [33].

The acetate diffusion length (L_D, in m) was calculated from the acetate kinetics, using Fick's law that yields to

$$L_D = \sqrt{D/k} = \sqrt{D\tau_{ct}} \quad \text{Eq.6}$$

in which the acetate diffusion coefficient in EABfs ($D = 2.2 \times 10^{-10}$ m^2 s^{-1}) was taken from [34].

The diffusion lengths ranged between 3 and 8 μm for all the intermittent EABfs. Considering a cylindrical *Geobacter* bacteria with 2 × 0.5 μm size [35], these penetration lengths suggest that only the top 4 to 16 layers of microorganisms in the EABfs had acetate available (assuming a vertical and horizontal orientation of the microorganisms in the EABf, respectively). As previously described for the acetate consumption rates, no clear relation between the acetate penetration lengths and the measured current densities and the EABfs thicknesses could be found (Figure C2, in Appendices). These lengths were much smaller than the measured EABf thicknesses that reached values of up to 60 μm, emphasizing that once a thick EABfs developed on the anode surface, most of the EABf layers have no access to acetate and therefore, only the top layers can oxidize acetate and produce current. These results suggest that to obtain higher currents, electrodes need to be engineered to maximize the fraction of EABfs with access to acetate, for instance by developing porous anodes or improving the acetate diffusion and mixing within the biofilm.

Finally, it has been shown here that while the fast electron transfer time from acetate oxidation determines the fraction of the EABf that contributes to the current production, the slow diffusion time of acetate (τ_d) – approximately 100 times slower than τ_{ct} – determines the time needed to reach a new equilibrium in the EABf after the successive potential steps applied during the intermittent measurements. This difference between τ_d and τ_{ct} means that acetate was consumed faster than it diffuses inside the EABfs, limiting the amount of EABf that was fed with acetate and thus the fraction of EABfs that was active. However, even though both the fast acetate consumption rate in the EABfs and the acetate diffusion lengths in the EABfs were shorter than the thickness of the EABf on the anode, these were not the only parameters contributing to the measured current density.

3.4. Concentration of charge carriers and current density

For a better understanding of the relationship between the current generated by the EABfs and their capacitance (C_{bio}), the number of charge carriers in the EABfs (n) was estimated using

$$C_{bio} = q \times \frac{dn}{dV} \rightarrow n \approx n_0 + \frac{C_{bio} \times \Delta V}{q} \quad \text{Eq.7}$$

in which q is the charge of one electron (-1.6×10^{-19} C) and ΔV is the change in potential during EIS measurements (two times the amplitude of the AC signal, 20 mV).

The number of charge carriers, n, in the EABfs is of crucial importance for electron transfer [24,36] and it was thus considered as one of the parameters that could be limiting and consequently, determining the measured current densities. As previously described in EIS studies [15], n is related to the capacitance of the EABf and it indicates the number of charge carriers present in the EABfs. These charge carriers (e.g., cytochromes) are redox compounds that facilitate the storage and the transfer of electrons derived from the consumed acetate through the

EABfs matrix towards the anode. These charge carriers are present in the EABf fraction that has access to acetate, but also in the lower layers of EABfs that are acetate depleted because these layers are also conductive [37,38].

Using Equation (7), the number of charge carriers in the EABf matrix was found to be in the order of magnitude of 10^{15} and fluctuated between 10^{14} and 10^{15} when the EABf thickness on the anode was approximately 10–30 μm. When thicker EABf developed on the anode, this number remained roughly constant at 10^{15}, meaning that the number of charge carriers did not accompany EABf growth. This has an important effect on the electron transfer rates in EABfs as more charge carriers are linked to higher EABf conductivities. Therefore, R_{bio} increased with increasing EABf thicknesses. This independence on the number of charge carriers and the thickness of EABfs on the anode could have been caused by the acetate limitations (as mentioned before), suggesting that not all the charge carriers present in the EABf were reduced. More details on the number of charge carriers and R_{bio} can be found in Figure D1, in Appendices.

The concentration of charge carriers in the EABfs was calculated for 1) the active EABfs, considering the EABf thickness that was not acetate limited using previously estimated acetate diffusion lengths and the FTO area, and 2) for the whole EABf, considering the total EABf thickness measured on the electrode and the FTO area. In Fig. 7, the current density produced by the intermittent EABfs is shown as a function of the concentration of charge carriers in both the acetate oxidizing fraction of the EABfs as well as the total measured EABfs thickness (in moles of charge carriers per m^3 of active/measured EABf, after dividing by Avogadro's number).

This figure shows that higher current densities are linked to higher concentrations of charge carriers in the EABfs. The two different slopes observed in this figure show that the concentration of charge carriers in the total volume of the EABfs was lower than the concentration of charge carriers in the active volume of the EABfs, which has to do with the thinner thicknesses of the EABfs measured on the anode when compared to the estimated acetate diffusion lengths (Figure D2, in Appendices). However, due to acetate limitations which could have resulted in an underestimation of C_{bio}, and thus the number of charge carriers, the concentration of charge carriers provides a more accurate relation with the current density when compared to the relation between the C_{bio} and the current density (Figure D3, in Appendices).

When normalizing by the molarity of heme groups (present in cytochromes), and the protein content in the cells present in the EABf (Equation D1, in Appendices), the concentration of charge carriers calculated in the total volume of the EABfs accounted for roughly 10^6 $protein_{heme}\ g_{cell}^{-1}$ when a current density of 1 A m^{-2} was measured and increased up to 10^7 $protein_{heme}\ g_{cell}^{-1}$ when current densities higher than 2 A m^{-2} were measured. Considering that each heme protein can store one electron, these results are in the same range of electron storage capacity previously reported for intermittent EABfs and for suspended cells of *Geobacter sulfurreducens* (both in the order of 10^7) [33,39].

4. Conclusions and outlook

EIS is a non-destructive electrochemical technique that allows to study and characterize EABfs. The combination of transient measurements in intermittent EABfs and EIS allowed to identify that while the diffusion dominates the long-term stabilization of the EABfs response, the produced current is dominated by the fast rate of acetate consumption which occurs on the top layers of the EABfs. This explains why despite the increasing EABf thicknesses, the acetate consumption, and therefore the produced current, becomes limited as acetate does not penetrate the inner layers of the EABfs. This overgrowth and negative effect on anodic currents suggest that optimal electrodes should be porous to increase the surface available for EABf growth and with pore diameters of hundreds of micrometers to avoid fast blocking of the pores by EABf growth. Besides, anode compartments with an optimized flow of anolyte are needed to ensure acetate is available in all the EABf layers.

Finally, EIS allowed to prove that the current density is related to the concentration of charge carriers in intermittent EABfs. Even though here used in intermittent EABfs, this analysis can also be used to study continuous EABfs and to better understand the effect of different anode potential regimes and acetate concentrations on the acetate oxidation rate and diffusion, and on the concentration of charge carriers in EABfs. This work shows the versatility and potential of EIS to study electro-active microorganisms that grow on electrodes and opens the door to further exploration on the use of this electrochemical technique to obtain more information on EABfs and hopefully increase BES performance.

Funding

This work was supported by the "Resource Recovery" theme of Wetsus; and Dutch Research Council (NWO) [project "Understanding and controlling electron flows in electro-active biofilms" with project number 17516 that is part of the research program Vidi].

CRediT authorship contribution statement

João Pereira: Conceptualization, Methodology, Investigation, Formal analysis, Writing – original draft. **Yuniki Mediayati:** Methodology, Investigation. **Tom Sleutels:** Conceptualization, Writing – review & editing. **Francisco Fabregat-Santiago:** Conceptualization, Formal analysis, Writing – review & editing. **Annemiek ter Heijne:** Conceptualization, Writing – review & editing, Supervision, Project administration, Funding acquisition.

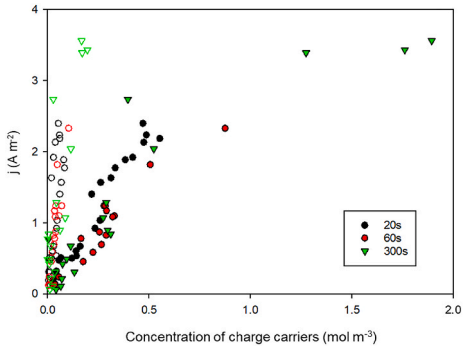

Fig. 7. Measured current density for the intermittent EABfs as a function of the calculated concentration of charge carriers in the volume of active EABf ($n/(L_D \times A_{FTO})$ – filled circles, and in the measured EABf volume ($n/(L_{bio} \times A_{FTO})$) – open circles. Higher current densities are linked to higher concentrations of charge carriers in the EABf.

Declaration of competing interest

The authors declare that they have no known competing financial interests or personal relationships that could have appeared to influence the work reported in this paper.

Data availability

The data will be made available after publication at doi: 10.4121/315b5fdb-c361-4bfd-ba7a-962870fe5c18. This link has been included in the manuscript

Acknowledgements

This work was performed in the cooperation framework of Wetsus, European Centre of Excellence for Sustainable Water Technology (www.wetsus.nl). Wetsus is co-funded by the Dutch Ministry of Economic Affairs and Ministry of Infrastructure and Environment, the European Union Regional Development Fund, the Province of Fryslân, and the Northern Netherlands Provinces. The authors thank the participants of the research theme "Resource Recovery" for the fruitful discussions and their financial support. This publication is part of the project "Understanding and controlling electron flows in electro-active biofilms" with project number 17516 of the research program Vidi which is (partly) financed by the Dutch Research Council (NWO). FF-S wants to acknowledge Ministerio de Economía y Competitividad (MINECO) from Spain under ECOCAT project PID2020-116093RB-C41 for financial support.

Appendix A. Supplementary data

Supplementary data to this article can be found online at https://doi.org/10.1016/j.jpowsour.2023.233725.

References

[1] B. Erable, N.M. Duţeanua, M.M. Ghangrekar, C. Dumas, K. Scott, Application of electro-active biofilms, Biofouling 26 (2010) 57–71, https://doi.org/10.1080/08927010903161281.
[2] B.E. Logan, R. Rossi, A. Ragab, P.E. Saikaly, Electroactive microorganisms in bioelectrochemical systems, Nat. Rev. Microbiol. 17 (2019) 307–319, https://doi.org/10.1038/s41579-019-0173-x.
[3] C. Santoro, C. Arbizzani, B. Erable, I. Ieropoulos, Microbial fuel cells: from fundamentals to applications. A review, J. Power Sources 356 (2017) 225–244, https://doi.org/10.1016/j.jpowsour.2017.03.109.
[4] H.V.M. Hamelers, A. Ter Heijne, T.H.J.A. Sleutels, A.W. Jeremiasse, D.P.B.T. B. Strik, C.J.N. Buisman, New applications and performance of bioelectrochemical systems, Appl. Microbiol. Biotechnol. 85 (2010) 1673–1685, https://doi.org/10.1007/s00253-009-2357-1.
[5] R. Kiran, S.A. Patil, Microbial electroactive biofilms, ACS (Am. Chem. Soc.) Symp. Ser. 1323 (2019) 159–186, https://doi.org/10.1021/bk-2019-1323.ch008.
[6] C.A. Ramírez-Vargas, A. Prado, C.A. Arias, P.N. Carvalho, A. Esteve-Núñez, H. Brix, Microbial electrochemical technologies for wastewater treatment: principles and evolution from microbial fuel cells to bioelectrochemical-based constructed wetlands, Water (Switzerland) 10 (2018) 1–29, https://doi.org/10.3390/w10091128.
[7] G.D. Saratale, R.G. Saratale, M.K. Shahid, G. Zhen, G. Kumar, H.S. Shin, Y.G. Choi, S.H. Kim, A comprehensive overview on electro-active biofilms, role of exo-electrogens and their microbial niches in microbial fuel cells (MFCs), Chemosphere 178 (2017) 534–547, https://doi.org/10.1016/j.chemosphere.2017.03.066.
[8] F. Harnisch, K. Rabaey, The diversity of techniques to study electrochemically active biofilms highlights the need for standardization, ChemSusChem 5 (2012) 1027–1038, https://doi.org/10.1002/cssc.201100817.
[9] S.M. de Smit, C.J.N. Buisman, J.H. Bitter, D.P.B.T.B. Strik, Cyclic voltammetry is invasive on microbial electrosynthesis, Chemelectrochem 8 (2021) 3384–3396, https://doi.org/10.1002/celc.202100914.
[10] F. Harnisch, S. Freguia, A basic tutorial on cyclic voltammetry for the investigation of electroactive microbial biofilms, Chem. Asian J. (2012), https://doi.org/10.1002/asia.201100740.
[11] D. Millo, An electrochemical strategy to measure the thickness of electroactive microbial biofilms, Chemelectrochem 2 (2015) 288–291, https://doi.org/10.1002/celc.201402425.
[12] Z. He, F. Mansfeld, Exploring the use of electrochemical impedance spectroscopy (EIS) in microbial fuel cell studies, Energy Environ. Sci. 2 (2009) 141–240, https://doi.org/10.1039/b814914c.
[13] S. Jung, Impedance analysis of Geobacter sulfurreducens PCA, Shewanella oneidensis MR-1, and their coculture in bioeletrochemical systems, Int. J. Electrochem. Sci. 7 (2012) 11091–11100.
[14] A. ter Heijne, O. Schaetzle, S. Gimenez, L. Navarro, B. Hamelers, F. Fabregat-Santiago, Analysis of bio-anode performance through electrochemical impedance spectroscopy, Bioelectrochemistry 106 (2015) 64–72, https://doi.org/10.1016/j.bioelechem.2015.04.002.
[15] A. ter Heijne, D. Liu, M. Sulonen, T. Sleutels, F. Fabregat-Santiago, Quantification of bio-anode capacitance in bioelectrochemical systems using Electrochemical Impedance Spectroscopy, J. Power Sources 400 (2018) 533–538, https://doi.org/10.1016/j.jpowsour.2018.08.003.
[16] A. ter Heijne, M.A. Pereira, J. Pereira, T. Sleutels, Electron storage in electroactive biofilms, Trends Biotechnol. 39 (2020) 34–42, https://doi.org/10.1016/j.tibtech.2020.06.006.
[17] E. Zhang, Q. Yu, Y. Zhang, K. Scott, G. Diao, The effect of intermittent limiting anodic current stimulation on the electro activity of anodic biofilms, J. Adv. Chem. Eng. 7 (2017) 1–7, https://doi.org/10.4172/2090-4568.1000174.
[18] J. Pereira, G. Wang, T. Sleutels, B. Hamelers, A. ter Heijne, Maximum thickness of non-buffer limited electro-active biofilms decreases at higher anode potentials, Biofilms 4 (2022), 100092, https://doi.org/10.1016/j.bioflm.2022.100092.
[19] J. Pereira, S. Pang, C. Borsje, T. Sleutels, B. Hamelers, A. ter Heijne, Real-time monitoring of biofilm thickness allows for determination of acetate limitations in bio-anodes, Bioresour. Technol. Rep. 18 (2022), 101028, https://doi.org/10.1016/j.biteb.2022.101028.
[20] R.S. Renslow, J.T. Babauta, P.D. Majors, H. Beyenal, Diffusion in biofilms respiring on electrodes, Energy Environ. Sci. 6 (2013) 595–607, https://doi.org/10.1039/c2ee23394k.
[21] H.-S. Lee, C.I. Torres, B.E. Rittmann, Effects of substrate diffusion and anode potential on kinetic parameters for anode-respiring bacteria, Environ. Sci. Technol. 43 (2009) 7571–7577.
[22] C.I. Torres, A.K. Marcus, B.E. Rittmann, Proton transport inside the biofilm limits electrical current generation by anode-respiring bacteria, Biotechnol. Bioeng. 100 (2008) 872–881, https://doi.org/10.1002/bit.21821.
[23] J. Pereira, Y. Mediayati, H.P.J. van Veelen, H. Temmink, T. Sleutels, B. Hamelers, A. ter Heijne, The effect of intermittent anode potential regimes on the morphology and extracellular matrix composition of electro-active bacteria, Biofilms 4 (2021), 100064, https://doi.org/10.1016/j.bioflm.2021.100064.
[24] X. Zhang, A. Prévoteau, R.O. Louro, C.M. Paquete, K. Rabaey, Periodic polarization of electroactive biofilms increases current density and charge carriers concentration while modifying biofilm structure, Biosens. Bioelectron. 121 (2018) 183–191, https://doi.org/10.1016/j.bios.2018.08.045.
[25] S.D. Molenaar, T. Sleutels, J. Pereira, M. Iorio, C. Borsje, J.A. Zamudio, F. Fabregat-Santiago, C.J.N. Buisman, A. Ter Heijne, In situ biofilm quantification in bioelectrochemical systems by using optical coherence tomography, ChemSusChem 11 (2018) 2171–2178, https://doi.org/10.1002/cssc.201800589.
[26] DSMZ, 141. Methanogenium medium (H2/CO2) [WWW Document]. URL, https://www.dsmz.de/microorgan-isms/medium/pdf/DSMZ_Medium141.pdf, 2017.
[27] J. Pereira, S. de Nooy, T. Sleutels, A. ter Heijne, Opportunities for visual techniques to determine characteristics and limitations of electro-active biofilms, Biotechnol. Adv. 60 (2022), 108011, https://doi.org/10.1016/j.biotechadv.2022.108011.
[28] R.S. Renslow, J.T. Babauta, P.D. Majors, H. Beyenal, Diffusion in biofilms respiring on electrodes, Energy Environ. Sci. 6 (2013) 595–607, https://doi.org/10.1039/c2ee23394k.
[29] C.I. Torres, A.K. Marcus, B.E. Rittmann, Proton transport inside the biofilm limits electrical current generation by anode-respiring bacteria, Biotechnol. Bioeng. 100 (2008) 872–881, https://doi.org/10.1002/bit.21821.
[30] M. García-Batlle, J. Mayén Guillén, M. Chapran, O. Baussens, J. Zaccaro, J. M. Verilhac, E. Gros-Daillon, A. Guerrero, O. Almora, G. Garcia-Belmonte, Coupling between ion drift and kinetics of electronic current transients in MAPbBr3 single crystals, ACS Energy Lett. 7 (2022) 946–951, https://doi.org/10.1021/acsenergylett.1c02578.
[31] D. Sun, J. Chen, H. Huang, W. Liu, Y. Ye, S. Cheng, The effect of biofilm thickness on electrochemical activity of Geobacter sulfurreducens, Int. J. Hydrogen Energy 41 (2016) 16523–16528, https://doi.org/10.1016/j.ijhydene.2016.04.163.
[32] L. Martinez Ostormujof, S. Teychené, W. Achouak, S. Fochesato, M. Bakarat, I. Rodriguez-Ruiz, A. Bergel, B. Erable, Systemic analysis of the spatiotemporal changes in multi-species electroactive biofilms to clarify the gradual decline of current generation in microbial anodes, Chemelectrochem 10 (2023), https://doi.org/10.1002/celc.202201135.
[33] P.S. Bonanni, G.D. Schrott, L. Robuschi, J.P. Busalmen, Charge accumulation and electron transfer kinetics in Geobacter sulfurreducens biofilms, Energy Environ. Sci. 5 (2012) 6188–6195, https://doi.org/10.1039/c2ee02672d.
[34] J. Pereira, G. Wang, T. Sleutels, B. Hamelers, A. ter Heijne, Maximum thickness of non-buffer limited electro-active biofilms decreases at higher anode potentials, Biofilm 4, https://doi.org/10.2139/ssrn.4200901, 2022.
[35] F. Caccavo, D.J. Lonergan, D.R. Lovley, M. Davis, J.F. Stolz, M.J. Mcinerneyl, Geobacter sulfurreducens sp. nov., a Hydrogen and Acetate Oxidizing dissimilatory metal reducing microorganism, Appl. Environ. Microbiol. 60 (1994) 3752–3759.
[36] R. Linssen, T. Slinkert, C.J.N. Buisman, J.B.M. Klok, A. ter Heijne, Anaerobic sulphide removal by haloalkaline sulphide oxidising bacteria, Bioresour. Technol. 369 (2023), 128435, https://doi.org/10.1016/j.biortech.2022.128435.

[37] H.S. Lee, Electrokinetic analyses in biofilm anodes: ohmic conduction of extracellular electron transfer, Bioresour. Technol. 256 (2018) 509–514, https://doi.org/10.1016/j.biortech.2018.02.002.
[38] D.R. Lovley, D.J.F. Walker, Geobacter protein nanowires, Front. Microbiol. 10 (2019), https://doi.org/10.3389/fmicb.2019.02078.
[39] A. Esteve-Núñez, J. Sosnik, P. Visconti, D.R. Lovley, Fluorescent properties of c-type cytochromes reveal their potential role as an extracytoplasmic electron sink in Geobacter sulfurreducens, Environ. Microbiol. 10 (2008) 497–505, https://doi.org/10.1111/j.1462-2920.2007.01470.x.